Int. J. Heat Mass Transfer. Vol. 28, No. 4, pp. 795–806, 1985
Printed in Great Britain

0017-9310/85 $3.00 + 0.00

Boiling heat transfer and critical heat flux in high-speed rotating liquid films

I. A. MUDAWWAR,* M. A. EL-MASRI, C. S. WU and J. R. AUSMAN-MUDAWWAR
Department of Mechanical Engineering, Massachusetts Institute of Technology, Cambridge, MA 02139, U.S.A.

(*Received 2 July 1984 and in final form 22 October 1984*)

Abstract— Boiling heat transfer measurements were obtained with water films in radial rotating channels. The boiling curve was found to resemble that for pool boiling of water. The critical heat flux (CHF) increased with pressure as well as rotational speed. A CHF model based upon the balance between the Coriolis forces and the vapor drag acting upon drops formed from the shattered film is presented. It facilitates the successful correlation of the data using a single empirical constant.

1. INTRODUCTION

BOILING liquid films are of paramount importance in several technological applications. Examples include annular two-phase flow heat exchangers, laser mirror cooling and one proposed method for water-cooling turbine blades. In the latter case, which is the motivation of our present analysis, water is driven by centrifugal forces in the radial direction inside the blade cooling passages. Coriolis forces, on the other hand, tend to maintain the flow in the form of a very thin film covering only one side of the coolant channel. Fully-developed flow is determined by a balance between centrifugal and shear forces. An analogy can be drawn between this configuration and inclined-plane non-rotating gravity-driven films. Both are characterized by a driving body force in the flow direction, together with a normal component which plays a less significant role in fully-developed single-phase flow. It should be mentioned that unlike the non-rotating configuration, the Coriolis (or normal) component in rotating systems is not a constant but depends on the flow field. This difference becomes significant during severe boiling, where the Coriolis force plays a major role in defining the trajectory of the splashed liquid film.

During the last decade, Japanese researchers published extensive boiling and CHF studies on high speed liquid films. In 1972, Toda and Uchida [1] presented their experimental findings for liquid-film jets in the range 2–10 m s^{-1}. The flow was driven by a rectangular nozzle over a square heater (30 × 30 mm). Boiling data were correlated by the following empirical equation:

$$q \propto (T_w - T_{sat})^{1.42}. \qquad (1)$$

The CHF was reported to occur as a result of a 'jump phenomenon' where the greater part of the film was pushed away at an angle to the heater surface due to the large vapor flux generated by vigorous boiling. Katto and Kunishiro [2] later conducted several boiling and CHF experiments with a small impingement liquid jet at the center of an 11-mm diam. copper disc where the film flow was established radially outward. They noticed a monotonic increase in the CHF with jet speed. In a more recent paper by Katto and Monde [3], high speed photographs of the burnout process revealed that the 'jump phenomenon' occurred in the form of splashed droplets rather than a liquid continuum. In an attempt to obtain clear two-dimensional optical studies of the CHF phenomenon, Katto and Ishii [4] carried out several tests with plane jets over rectangular heated surfaces. CHF data for water, Freon-113 and trichloroethane using three different heater lengths (10, 15 and 20 mm) were correlated by the following equation:

$$\frac{q_M}{\rho_v h_{fg} u_0} = 0.0164\left(\frac{\rho_l}{\rho_v}\right)^{0.867}\left(\frac{\sigma}{\rho_l u_0^2 L}\right)^{1/3} \qquad (2)$$

where u_0 is the inlet jet velocity and L is the length of the heater. Katto and Shimizu [5] also did further tests with the impinging jet experiment using Freon-12 at relatively high pressures (6–27.9 bars), together with more atmospheric-pressure data for water and Freon-113. For the low pressure range, they correlated their data in the following form:

$$\frac{q_M}{\rho_v h_{fg} u_0} = 0.188\left(\frac{\rho_l}{\rho_v}\right)^{0.614}\left(\frac{\sigma}{\rho_l u_0^2 D}\right)^{1/3} \qquad (3a)$$

where D is the diameter of the heater. For the high pressure range, they recommended a different correlation characterized by stronger dependence on surface tension as shown by the following equation:

$$\frac{q_M}{\rho_v h_{fg} u_0} = 1.18\left(\frac{\rho_l}{\rho_v}\right)^{0.614}\left(\frac{\sigma}{\rho_l u^2 D}\right)^{1/2}. \qquad (3b)$$

In an attempt to explain the CHF dependence exhibited by equations (3a) and (3b), Lienhard and Eichhorn [6] assumed that burnout occurs when the kinetic energy of the vapor formed at the heater surface is transferred into surface energy required to form the droplets. Their analysis, however, introduced various

* Current address: Department of Mechanical Engineering at Purdue University, West Lafayette, IN 47907, U.S.A.

NOMENCLATURE

- a acceleration component in the flow direction, $\omega^2 R$, $g \sin\theta$
- a_n acceleration component normal to the flow direction, $2\omega u$, $g\cos\theta$
- C_D drag coefficient
- D diameter of heated disc, droplet diameter
- g acceleration due to gravity
- h convective heat transfer coefficient
- h_{fg} latent heat of vaporization
- h^* non-dimensional heat transfer coefficient, $(h\nu_l^{2/3})/k_l a^{1/3}$
- h_E^* non-dimensional evaporation heat transfer coefficient, $(h_E \nu_l^{2/3})/k_l a^{1/3}$
- h_H^* non-dimensional heat transfer coefficient in the absence of evaporation, $(h_H \nu_l^{2/3})/k_l a^{1/3}$
- k_l thermal conductivity of the saturated liquid
- L heater length
- P static pressure
- Pr Prandtl number
- q wall heat flux
- q_M critical heat flux (CHF)
- q_M^* non-dimensional CHF defined in equation (21)
- R radius of rotation
- Re film Reynolds number, $4\Gamma/\mu_l$
- T_s temperature of the free surface of the film
- T_{sat} saturation temperature corresponding to the operating static pressure
- T_w wall temperature
- u average film speed, Γ/δ
- u_i superficial vapor speed, $q_M/\rho_v h_{fg}$
- u_0 average film speed at the heater inlet.

Greek symbols

- Γ mass flow rate per unit film width
- ΔT_{sat} wall superheat
- ΔT_{sub} wall subcooling
- δ film thickness
- δ_0 initial film thickness
- θ inclination angle in non-rotating gravity-driven liquid films
- λ_E variable coefficient in equation (10)
- λ_H variable coefficient in equation (9)
- μ_l viscosity of the saturated liquid
- ν_l kinematic viscosity of the saturated liquid
- ρ_l density of the saturated liquid
- ρ_v density of the saturated vapor
- σ surface tension
- ω rotational speed.

unknown constants that had to be evaluated from experimental data.

Ueda *et al.* [7] attacked the CHF problem in vertical freely-falling films for a wide range of conditions. Their test section was a 58-cm long, 8-mm O.D. tube heated at its lower end. The CHF data were strongly affected by the Reynolds number (which determined the average film speed). For lower velocities, burnout occurred when dry patches started to form on the heater surface. For high film velocities, the CHF occurred after the liquid film separated from the surface in a manner similar to that reported by Toda and Uchida [1]. CHF results for this latter velocity range were in fair agreement with equation (2).

More recently, Baines [8, 9] conducted extensive two-dimensional inclined-plane film experiments over an 11.4×6.5 cm^2 heater section. The liquid was fed in either as a jet (through a rectangular nozzle) or by flowing freely from a reservoir located 1.45 m upstream of the heater. Using both water and Freon-113, Baines covered a film-speed range of 1–5 m s^{-1}. CHF results for both fluids were scattered between equation (2) and the pool boiling CHF given by

$$\frac{q_M}{\rho_v h_{fg}} = 0.15\left[\frac{\sigma g \cos\theta(\rho_l - \rho_v)}{\rho_v^2}\right]^{1/4}. \quad (4)$$

The departure of Baines' data from Katto and Ishii's [equation (2)] could only be explained by Baines' much larger length-to-thickness ratio. Nevertheless the CHF was also characterized by the 'jump phenomenon' and the splashing of liquid droplets. Baines presented a mechanistic model for the CHF based upon experimental observations. It starts with the assumption that prior to the CHF, the film will separate at a small angle from the leading edge. The heated surface, however, continues to be cooled adequately by the droplets that are ejected from the shattered film. As the heat flux is increased, the separation angle will also increase, throwing the ejected droplets further downstream from the surface. For a finite heater length, the CHF occurs when most of the droplets are ejected beyond the end of the heater. Baines' model gives the following CHF relation,

$$\frac{q_M}{\rho_v h_{fg} u_0} \propto \left(\frac{\rho_l}{\rho_v}\right)^{2/3}\left(\frac{\sigma}{\rho_l u_0^2 L}\right)^{1/3} \quad (5)$$

which is somewhat similar to equation (2).

All previous heat transfer data for rotating films were obtained by the open-circuit blade cooling test facility at General Electric Company [10–12]. This facility was used to predict the CHF in water-cooled turbine blades. Blade heating by the hot gas was simulated by several cartridge heaters embedded in an 11-cm long copper cylinder surrounding the coolant channel. The mean radius of rotation used was 0.84 m which produced up to 1.1×10^5 m s^{-2} of centrifugal acceleration (at 1100–3600 rpm). Most data were obtained at atmospheric pressure for water films inside circular tubes rather than two-dimensional channels. Since no measurement of the film coverage of the cross section was possible, heat transfer coefficients could not be determined. Rather, they were calculated using Dukler's [13] theoretical evaporation heat transfer coefficients for freely-falling turbulent liquid films, and the circumferential wetted fraction was back-calculated. The blade-cooling test facility, however, failed to produce reliable estimates of the CHF in the absence of any prior knowledge about the exact wetted area during severe boiling.

The CHF problem in rotating liquid films was addressed theoretically by El-Masri and Louis [14]. They chose the Kutateladze [15] separation model as a physical explanation for CHF. In this model, the CHF is assumed to occur when the kinetic energy of the vapor stream normal to the wall becomes capable of ejecting the liquid remaining between the tightly packed bubbles at the heater surface. Their modified separation criterion was presented in the form

$$\frac{q_M}{[h_{fg}\rho_l^{1/2}\rho_v^{1/2}v_l^{1/3}]a^{1/3}} = f(Re). \quad (6)$$

In light of the above discussion, one could draw the general conclusion that the physical nature of the CHF in non-rotating liquid films changes with the heater length. Since rotating films in gas turbine applications are characterized by large length-to-thickness ratios, a rotating-film CHF model should particularly address the long-heater limit. Development of such a model requires reliable two-dimensional CHF experimental data.

2. EXPERIMENTAL APPARATUS

The present experimental work studied the heat transfer characteristics of water films in two-dimensional rotating channels subject to variations of static pressure (1–5.41 atm), Reynolds number (7000–72,000), centrifugal acceleration (a/g = 36.5–460), and subcooling (0–24°C). Figure 1 shows a schematic diagram of the primary components of the rotating system. The test channel was mounted on a 34.3-cm O.D. rotating disc (shown on the left hand side of the figure). Pressurization occurred inside a 49.5-cm O.D. aluminum pressure chamber. The primary drive shaft (1.52 m long) was made of a 7.6-cm O.D. stainless steel rod. A 7.5 hp motor with a variable speed eddy-current clutch was used to spin the disc at speeds up to 1775 rpm. Electric power was introduced through water-cooled carbon brushes via two copper rings which transmitted the DC current to the rotating channel. Water was introduced axially from the external end of the shaft through a mechanical seal. A small nozzle at the end of the test section accelerated the flow in the form of an impingement jet onto the surface of a stagnation heater. This heater was placed at the center of the rotating disc to preheat the water to the saturation temperature. Finally the flow was diverted radially outward through a spiral passage into the test channel (see Fig. 2). The slip-ring assembly played the dual function of providing electric power to the stagnation heater as well as transmitting voltage signals from the heat transfer test channel to the external electronic circuitry.

The electric heater consisted of a 0.076-mm nichrome ribbon. The test channel was a thermally-optimized composite-wall structure (see Fig. 3) in which the metallic ribbon heater was shielded from the boiling surface. The rotating film was heated over a 12 ×

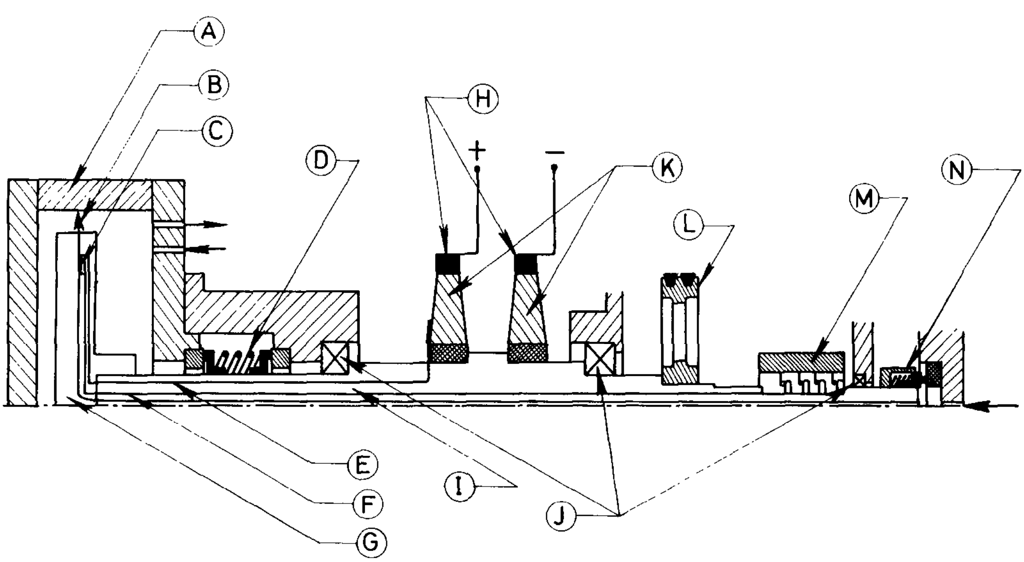

FIG. 1. Schematic view of the rotating system. A : pressure chamber ; B : liquid film ; C : CHF heater ; D : seal ; E : CHF power line ; F : stagnation heater electric cables and sensor wires ; G : rotating disc ; H : carbon brushes ; I : shaft ; J : bearings ; K : copper rings ; L : pulley ; M : slip-ring assembly ; N : inlet seal.

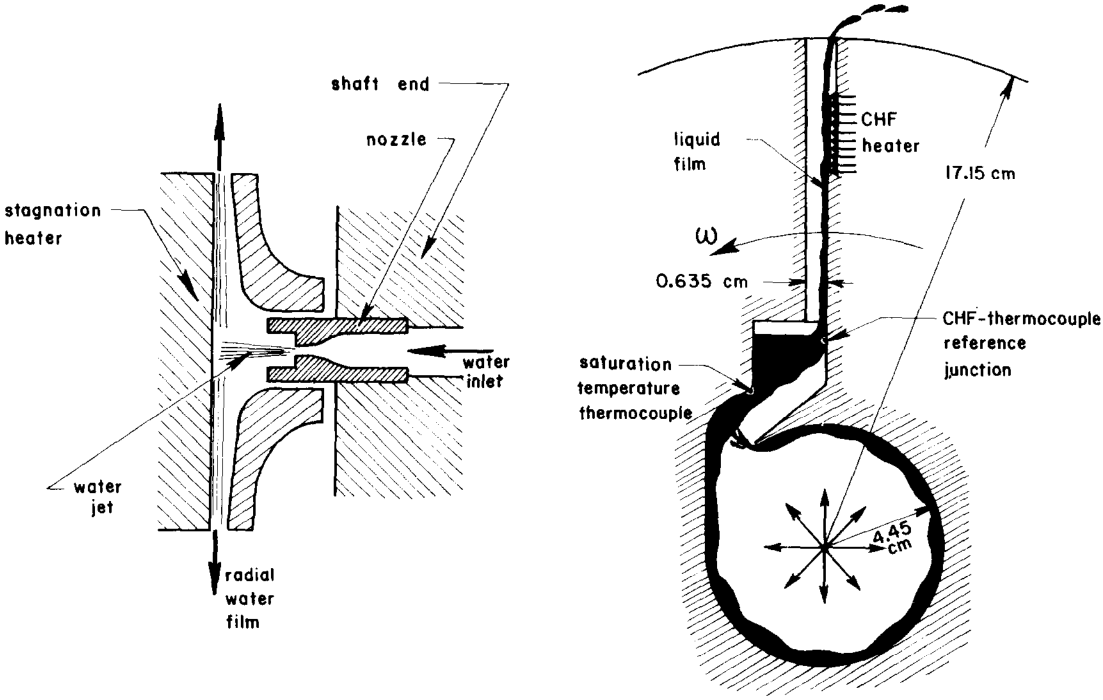

FIG. 2. Impingement jet flow against the surface of the stagnation heater and the spiral film flow inside the rotating disc.

6.35 mm^2 oxygen-free copper surface. To electrically insulate the ribbon from the copper surface, it was covered with a 0.53-mm boron nitride plate. This ceramic material combines the unique features of high thermal conductivity ($k > 40$ W m^{-1} $°C^{-1}$) and excellent electrical insulation. As shown in Fig. 3, two thermocouples were embedded in the copper block. These thermocouples played the dual role of monitoring the wall temperature as well as activating an external electronic protection circuit to shut off the heater power as soon as the CHF was detected. The extended copper body to the left of the heated wall in Fig. 3 provided some thermal capacitance which slowed down temperature excursions resulting from the CHF. Electric power was supplied through two stainless steel terminals. The electrical contact between

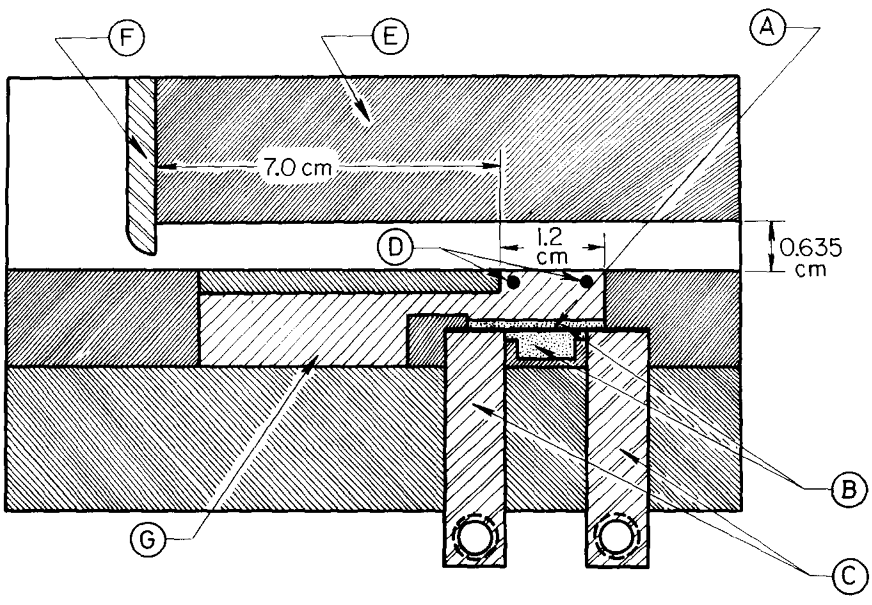

FIG. 3. Construction of the CHF probe. A: ribbon heater; B: boron nitride plates; C: stainless steel electric power terminals; D: thermocouples; E: G-7 plastic insulator (used in most of the probe pieces); F: nozzle plate; G: copper block.

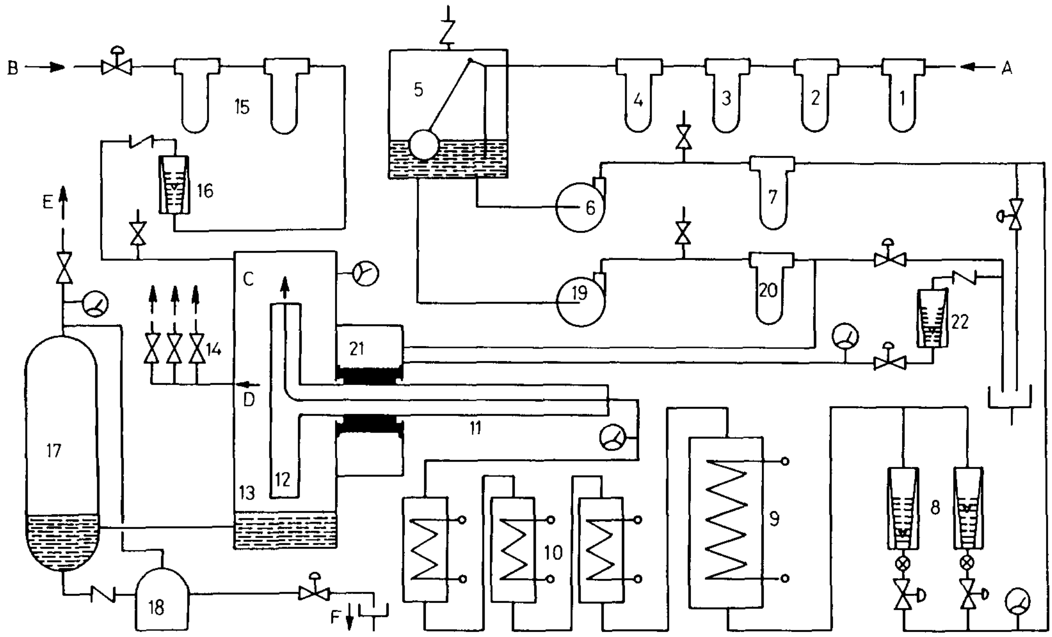

FIG. 4. Schematic diagram of the fluid delivery system. A: water inlet; B: air inlet; C: water and steam mixture; D: air and steam mixture; E: air and steam mixture; F: water drain. 1: 50-micron water filter; 2: 5-micron water filter; 3: de-ionizer; 4: activated charcoal filter; 5: water reservoir; 6: main water pump; 7: high-pressure water filter; 8: water flowmeters; 9: high power heater; 10: temperature-controlled heaters; 11: rotating shaft; 12: rotating disk; 13: pressure chamber; 14: pressure relief valves; 15: 5-micron air filters; 16: air flowmeter; 17: pressure stabilizer; 18: high-pressure water sump; 19: seal-water pump; 20: high-pressure water filter; 21: mechanical seal; 22: seal-water flowmeter.

these terminals and the ribbon was secured by high-temperature oven brazing. The main structure of the probe was built of G-7 plastic, a fiber-glass silicon-base high-temperature material characterized by low thermal conductivity ($k = 0.2$ W m^{-1} °C^{-1}) and considerable mechanical strength. The pressure inside the square shaped channel (6.35×6.35 mm^2) was equilibrated with the outside by a number of 1.59 mm holes (not shown in the figure) drilled along the side wall of the probe. Close alignment of the probe inserts was achieved through high machining accuracy (to within 0.0076 mm). Water was introduced to the probe in the form of a variable thickness wall jet (0.5–2.5 mm) through a stainless steel injection plate. The entire probe was mounted on the rotating disc with a surface-alignment accuracy of 0.025 mm in a plane normal to the axis of rotation. The water jet thinned out along the channel surface due to centrifugal acceleration ($\delta = 0.04$–0.52 mm) before being freely ejected in the radial direction. Accordingly, all heat transfer data were obtained with high length-to-thickness ratios (23–300).

Water was purified (see Fig. 4) and chemically deionized in four successive stages. At the end of the filtration process, water was accumulated inside a large atmospheric-pressure reservoir. Two high-pressure twin piston pumps supplied the desired water flow rates from the reservoir to the mechanical seal and the CHF probe. Before entering the shaft, the water was preheated in several stages. Most of the sensible heat addition occurred inside the high capacity electric preheater (up to 11 kW). The second preheating stage involved three smaller 1 kW heaters. Pre-shaft temperature control was maintained to within 3°C by a high-accuracy temperature controller. The main purpose of external preheating was to bring the water temperature as close as possible to the saturation level, thus reducing the heat load on the rotating stagnation heater.

Inside the pressure chamber, a portion of the liquid was vaporized into steam which mixed with air (used for pressurization), while the remaining water was transferred by gravity to a rejection trap. The gaseous mixture was then rejected via several high-capacity pre-calibrated relief valves. This fluid rejection scheme eliminated the possibility of re-condensation inside the test channel.

3. EXPERIMENTAL RESULTS

As shown in Figs. 5–8, the boiling data of rotating liquid films exhibit general similarity with static pool or forced convection boiling curves. Figure 5 displays the significance of subcooling on the CHF. As shown in this figure, 24°C of subcooling increased the CHF by 22%. Safe (lowest) estimates of the CHF could then only be obtained with saturated films. For this reason, most of the experiments were conducted with saturated flow. Figure 6 shows the variation in saturated boiling characteristics with pressure (1–5.41 atm). The CHF

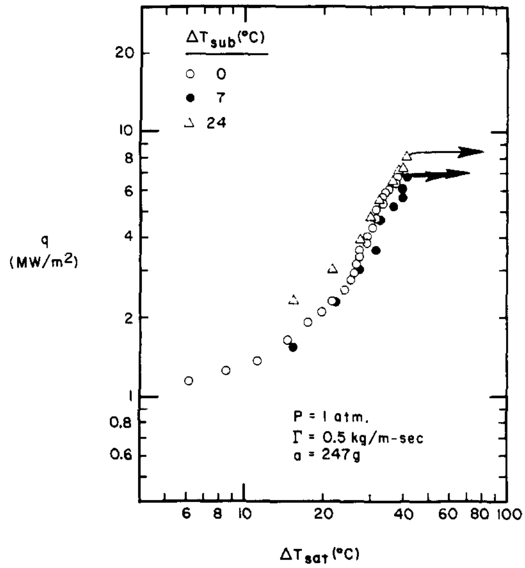

FIG. 5. Effect of subcooling on heat transfer.

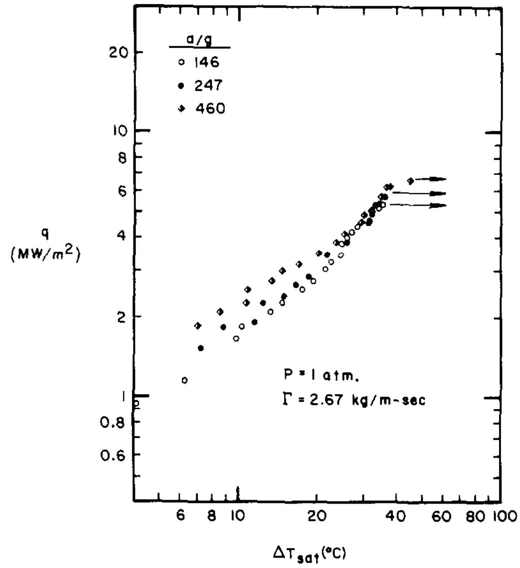

FIG. 7. Effect of rotation on heat transfer.

was substantially boosted with pressure (100% increase from 1 to 5.41 atm). Figure 7 shows similar effects resulting from higher rotational speeds ($a/g = 146$–460). The increase in the CHF, though not as significant, still displays a clear monotonic dependence on acceleration. Flow rate dependence, on the other hand, seems undefined (see Fig. 8). The forced convection part of the boiling curve is more sensitive to Reynolds number variations. This increase in the heat transfer coefficient with flow rate is also responsible for delayed incipient boiling.

4. ANALYSIS

Forced convection heat transfer

Predictions of heat transfer coefficients were previously presented in ref. [16] both for inclined-plane and rotating-film flows. Results were based on a semi-empirical turbulence model which was successful in predicting static-channel data published by several investigators. Two different coefficients were introduced for saturated rotating films, namely h_H^* and h_E^*. The first refers to the case of heating in which all the energy supplied is absorbed by the film. h_E^*, on the other hand, applies to evaporating films. From ref. [16]

$$h_H^* = \frac{q_w \nu_l^{2/3}}{(T_w - T_s) k_l a^{1/3}} = 0.069\ \lambda_H\, Re^{0.16}\, Pr^{0.475} \quad (7)$$

$$h_E^* = \frac{q_w \nu_l^{2/3}}{(T_w - T_{sat}) k_l a^{1/3}} = 0.042\ \lambda_E\, Re^{0.17}\, Pr^{0.53} \quad (8)$$

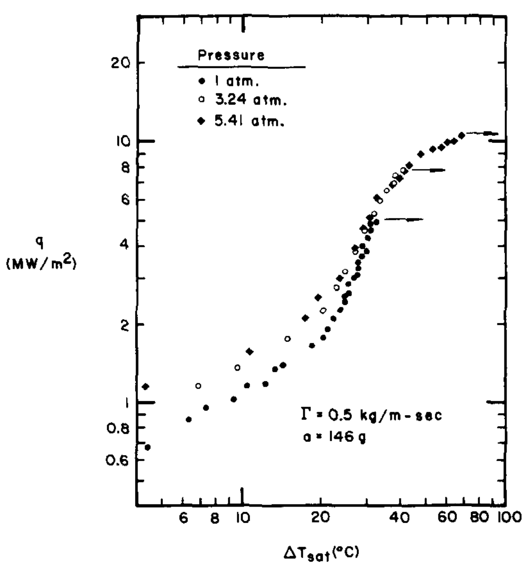

FIG. 6. Effect of pressure on heat transfer.

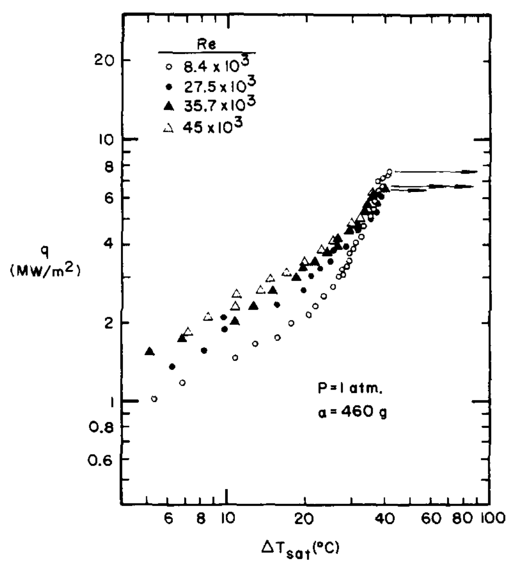

FIG. 8. Effect of flow rate on heat transfer.

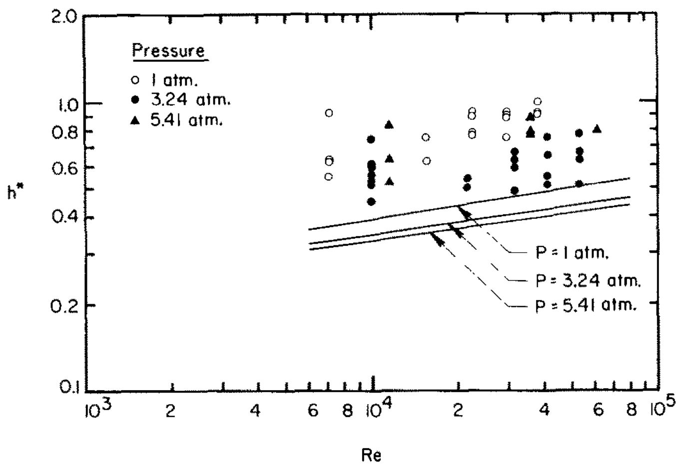

FIG. 9. Comparison of experimental and calculated heat transfer coefficient.

where

$$\lambda_{\mathrm{H}} = 1.335\, Pr^{-0.454}\, Re^{[0.145(Pr-0.3)^{0.2}-0.16]} \quad (9)$$

$$\lambda_{\mathrm{E}} = Pr^{-0.48}\, Re^{[0.18(Pr-0.3)^{0.18}-0.17]} \quad (10)$$

$$Re \equiv \frac{4\Gamma}{\mu_{1}}. \quad (11)$$

For a given set of operating conditions, the convective heat transfer coefficient (prior to boiling) depends on the length of the heater. At the entrance to the heated section, all the supplied energy is absorbed by the saturated film and no evaporation takes place. Accordingly, the surface temperature T_s is maintained at the saturation level while the wall temperature T_w keeps increasing. Once the temperature profile becomes fully developed, the heat transfer coefficient approaches h^*_{H}. Surface evaporation is then initiated and the profile develops further to the point where $h^* \to h^*_{\mathrm{E}}$. The saturated-film thermal flow regimes then include an entrance region where $h^* > h^*_{\mathrm{H}}$, a fully-developed heating region where $h^* = h^*_{\mathrm{H}}$, a developing evaporation region where $h^*_{\mathrm{E}} < h^* < h^*_{\mathrm{H}}$, and a fully-developed evaporation region where $h^* = h^*_{\mathrm{H}}$. Furthermore, since the film was very thin (0.04–0.52 mm), any wall roughness could have increased the heat transfer coefficient. Figure 9 shows the variation of h^* with Reynolds number for three different pressures. Despite the significant increase in h^* in the entrance, the data follow the same trend predicted by the turbulence model developed in ref. [16].

Fully-developed boiling

The rotating film heat transfer data reveal weak dependence of fully-developed boiling on pressure, flow rate or rotation. Figures 10–12 show only fully-developed boiling data points obtained from all the saturated-flow curves. The slope of the boiling curve is quite similar to the jet-flow results of Toda and Uchida [1], although our heat flux was generally higher. The

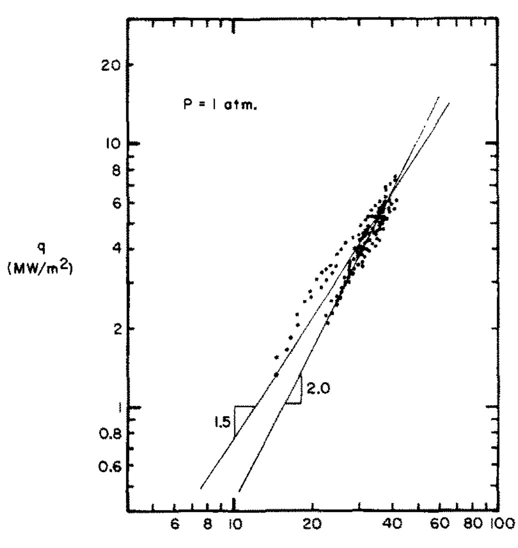

FIG. 10. Fully-developed boiling data at 1 atm.

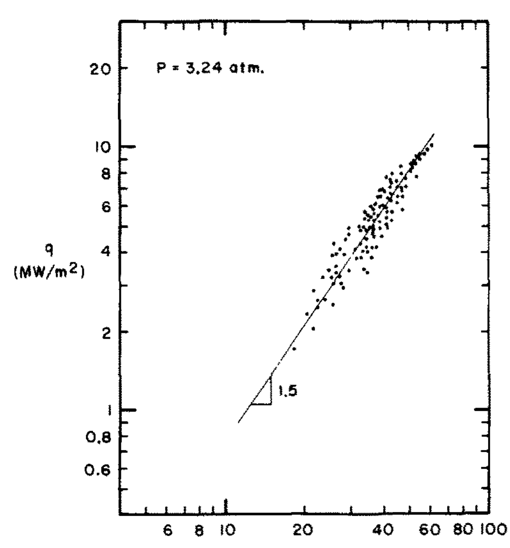

FIG. 11. Fully-developed boiling data at 3.24 atm.

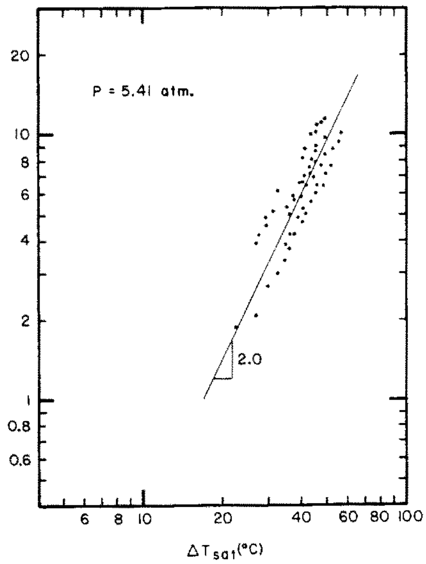

FIG. 12. Fully-developed boiling data at 5.41 atm.

rotating film data could be fairly correlated with an rms deviation of 0.87 MW m^{-2} by the empirical equation

$$q = 1.04 \times 10^4 (T_w - T_{sat})^{1.75} \tag{12}$$

where q is expressed in W m^{-2} and ΔT_{sat} in °C.

CHF model

In conventional multi-phase pipe-flow applications, continuity is bound by a known flow area. This is not the case, however, in liquid films since the flow area is itself a dependent variable. Reference [16] includes an attempt to simplify the boiling-film problem by pre-specifying basic physical assumptions regarding momentum vapor–liquid interaction at the wall and in the two-phase mixture. Numerical calculations for typical flow conditions, however, reveal that the void fraction increases substantially near the CHF (beyond 95% in our rotating-film case). This fact demonstrates the importance of introducing film-breakdown effects.

To acquire a better physical understanding of the CHF in liquid films, several simulation experiments were carried out by Baines [8] with non-rotating inclined-plane films. One set of his photographs of the film breakdown sequence is shown in Fig. 13. Baines noticed that the liquid film separated from the heater and formed individual droplets. Just prior to the CHF, the droplet removal rate from the heater surface becomes so excessive that it outweighed the rate of drop re-deposition so that no further wetting could be provided for the downstream end of the heater. Furthermore, for a given wall flux, large drops remain in the vicinity of the wall while a large population of much finer droplets is ejected further away from the

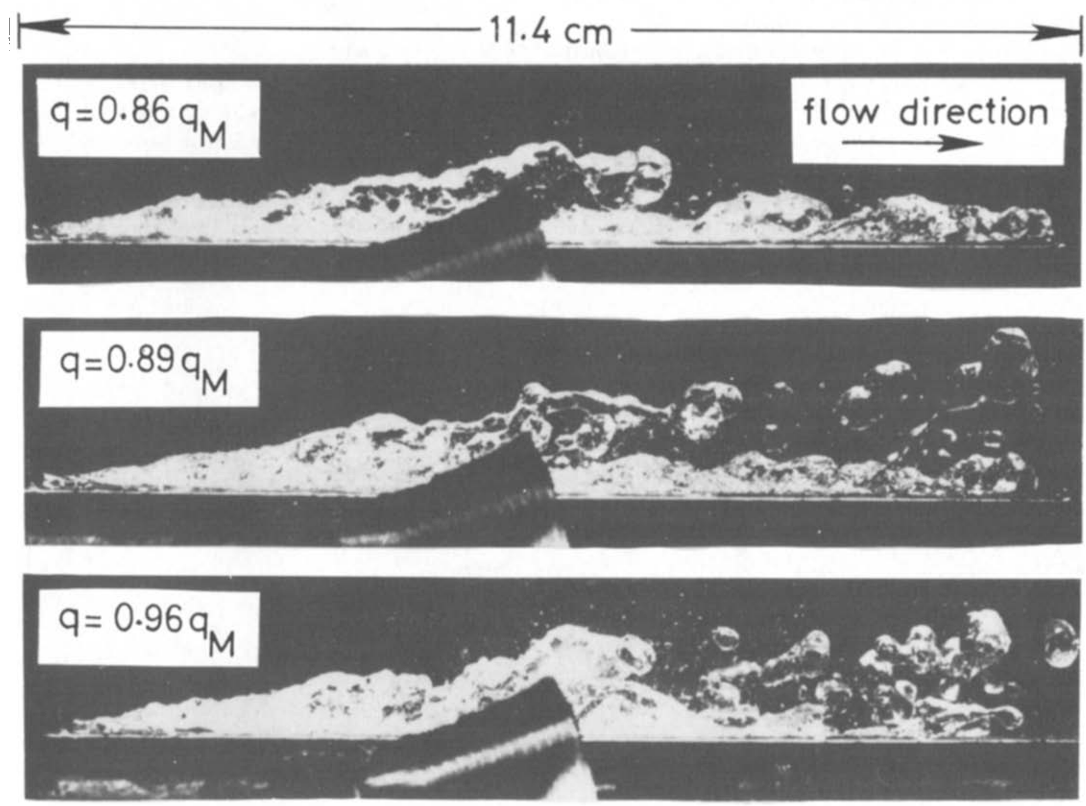

FIG. 13. Successive stages of film breakdown leading to CHF in inclined-plane water films obtained by Baines [8] (u_0 = 0.83 m s^{-1}, q_M = 1.252 MW m^{-2}). The object shown in the middle of each figure is external and did not interfere with the flow.

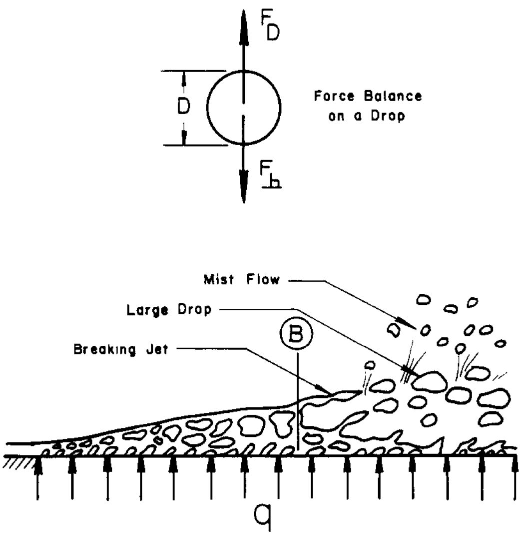

FIG. 14. Schematic representation of CHF.

surface. This process is represented schematically in Fig. 14. The liquid continuum is maintained until point B, beyond which it shatters and forms tiny jets which tend to break down further into droplets. For long heaters, breakdown occurs over a very short distance from the channel entrance. Beyond point B, vapor can no longer be entrained by the film. The CHF in this case is encountered as soon as the vapor drag overcomes the restoring body force (perpendicular to the flow direction) of the largest droplets. Equilibrium between these forces for a rotating channel is represented by the equation

$$C_D \frac{\pi D^2}{4} \frac{1}{2} \rho_v u_i^2 = (\rho_l - \rho_v) \frac{\pi}{6} D^3 a_n \tag{13}$$

where u_i is the superficial vapor velocity given by

$$u_i = \frac{q_M}{\rho_v h_{fg}}. \tag{14}$$

The maximum droplet size is determined by a critical Weber number beyond which the drops tend to rupture into a number of finer droplets. This criterion could be expressed in the form

$$\frac{\rho_v u_i^2 D}{\sigma} = \text{constant.} \tag{15}$$

Substituting equations (14) and (15) for u_i and D respectively, equation (13) (using constant C_D) reduces to the expression

$$q_M \propto \rho_v h_{fg} \left[\frac{(\rho_l - \rho_v) a_n \sigma}{\rho_v^2} \right]^{1/4}. \tag{16}$$

For inclined-channel flow, $a_n = g \cos \theta$. The

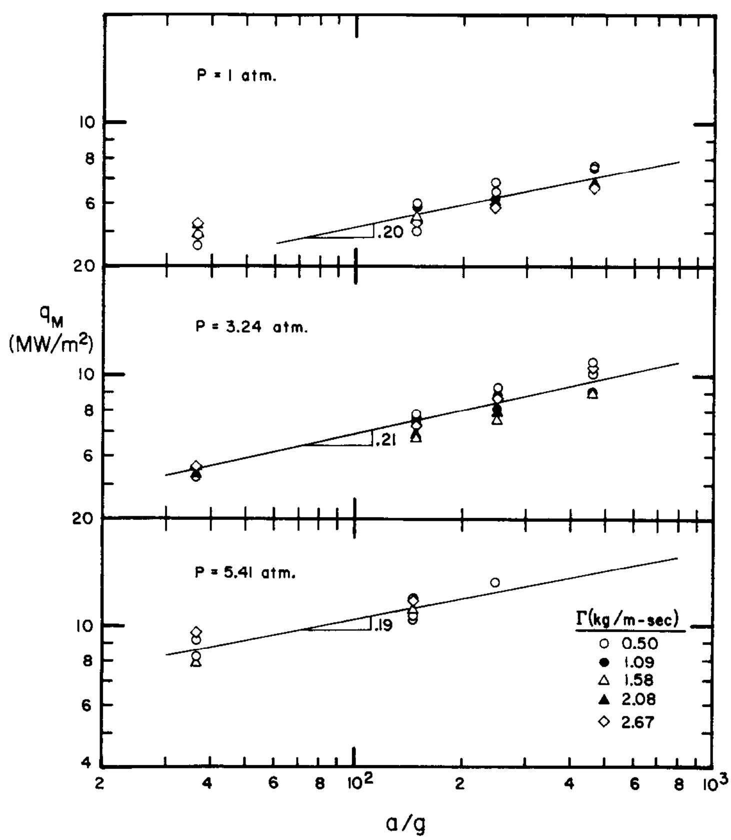

FIG. 15. Effect of centrifugal acceleration on CHF.

resultant CHF functional dependence becomes

$$q_{\mathrm{M}} \propto \rho_{\mathrm{v}} h_{\mathrm{fg}} \left[\frac{(\rho_{\mathrm{l}}-\rho_{\mathrm{v}}) g \cos \theta \sigma}{\rho_{\mathrm{v}}^2} \right]^{1/4}. \tag{17}$$

For a horizontal wall jet, the non-dimensional parameters of the above equation resemble those of the Kutateladze [17] and Zuber [18] correlations for the pool-boiling CHF despite the basic physical differences between the two cases. Furthermore, experimental results by Baines [8, 9] are in fair agreement with equation (17). This fact emphasizes the physical consistency of the present model.

In rotating films, the equivalent restoring force is the Coriolis component given by

$$a_{\mathrm{n}} = 2\omega u. \tag{18}$$

The average droplet velocity cannot be obtained directly in this case due to the complicated flow pattern. We may assume, however, that the acquired droplet speed is of the same order as the film it originated from. As a result of the intense vapor generation upstream of point B, the wall shear stress becomes negligible. From the conservation of mass and momentum, the average liquid speed at point B is equivalent to the inlet film velocity just upstream of the heated section. Based on Dukler's analysis of single-phase liquid films [13] (or from purely dimensional arguments),

$$\frac{\delta_0 a^{1/3}}{v_{\mathrm{l}}^{2/3}} = f(Re) \tag{19}$$

from which we obtain

$$\frac{u}{(v_{\mathrm{l}} a)^{1/3}} \sim \frac{u_0}{(v_{\mathrm{l}} a)^{1/3}} = f(Re). \tag{20}$$

Combining the above expressions with equations (16) and (18), our CHF model reduces to the following equation:

$$q_{\mathrm{M}}^* = \frac{q_{\mathrm{M}}}{\rho_{\mathrm{v}} h_{\mathrm{fg}} \left[\dfrac{(\rho_{\mathrm{l}}-\rho_{\mathrm{v}}) \sigma \omega (v_{\mathrm{l}} a)^{1/3}}{\rho_{\mathrm{v}}^2} \right]^{1/4}} = f(Re). \tag{21}$$

Since $a = \omega^2 R$, it follows that

$$q_{\mathrm{M}} \propto a^{0.208}. \tag{22}$$

The exponent in the above expression is very close to the slope of the best-fitted lines from our CHF data as shown in Fig. 15. This excellent agreement is demonstrated further by plotting all the CHF data according to equation (21) vs Reynolds number in Fig. 16. The entire results could be correlated by a single empirical equation

$$q_{\mathrm{M}}^* = 0.69 \tag{23}$$

with an rms deviation 0.099. The agreement of the data of equation (23) corroborates the physical consistency of the CHF model. As shown in Fig. 17, the present correlation results in values of CHF well above the predictions of El-Masri and Louis [equation (6)], whose model is based upon separation of the liquid film which does not necessarily result in CHF. Equation (23) applies only for long heaters (characterized by a large length-to-thickness ratio typical of the rotating-film experiments) where breakdown occurs near the upstream end of the heated section. Shorter heaters, on the other hand, are characterized by delayed breakdown, where B is closer to the downstream end. The CHF in this extreme limit is strongly dependent on the details of the breakdown process rather than the individual droplet behavior. This fact explains the departure of Baines' [8, 9] long-heater data from Katto and Ishii's [4] short-heater CHF correlation.

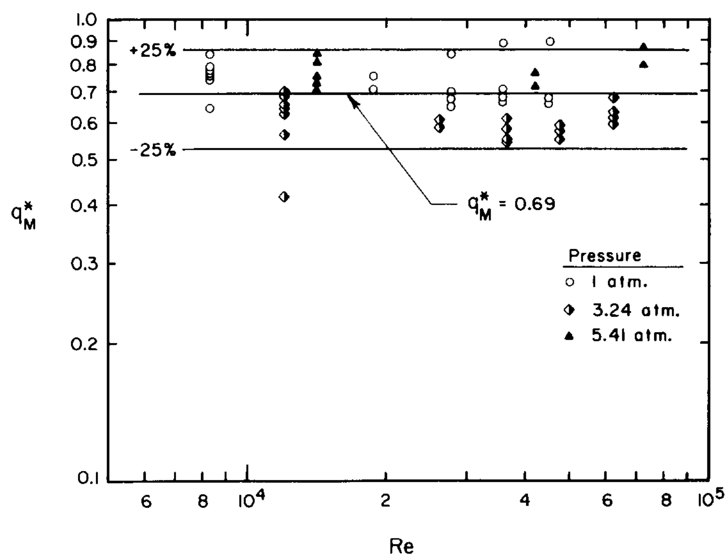

FIG. 16. CHF correlation based on the Coriolis-force model.

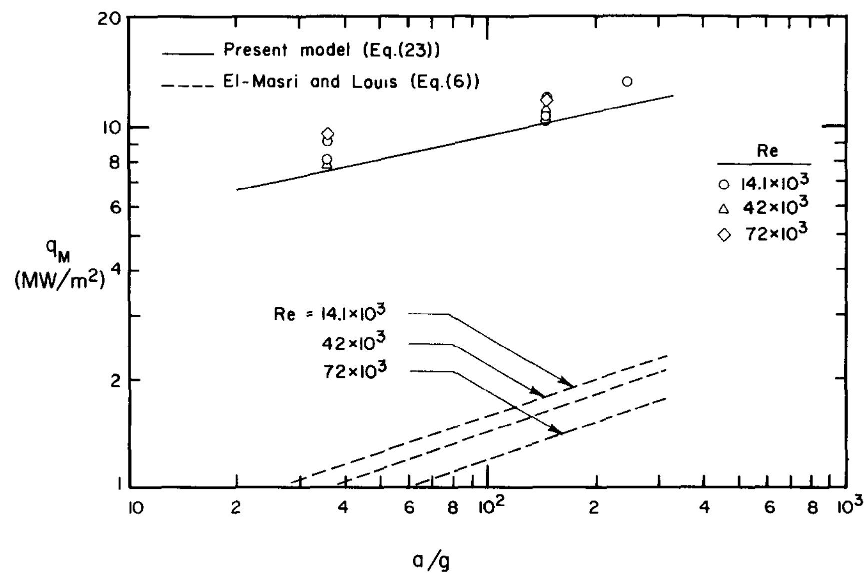

FIG. 17. Comparison of the present CHF correlation and El-Masri and Louis' [14] separation model with experimental data at 5.41 atm.

5. CONCLUSIONS

(1) The heat transfer coefficient for fully-developed boiling in rotating liquid films was found insensitive to variations in flow rate or centrifugal acceleration.

(2) Turbulent boundary-layer separation is not a sufficient physical description for the CHF in high-speed liquid films. Re-wetting can still be provided by broken three-dimensional droplet flow even after separation. The critical-flux level is encountered when the severe vapor drag normal to the boiling surface overcomes the restoring body forces (gravity or Coriolis) on these droplets.

(3) The CHF in liquid films over long heaters ($L/\delta_0 \gg 1$) depends on the individual downstream droplet behavior rather than the details of the film-breakdown process. For this reason, the short-heater CHF correlation of Katto and Ishii [equation (2)] should be avoided in these applications.

(4) The CHF in rotating liquid films increases both with pressure and centrifugal acceleration, but is insensitive to flow rate variations. The authors believe that the correlation given by equation (23) could be extended to a wide range of operating conditions because of the physical basis on which it is derived and its agreement with the data.

Acknowledgements—The authors acknowledge the partial support provided by each of the following organizations: U.S. Department of Energy, contract E(49-18)-2295; NSF, grant MEA-8017416; and the MIT Energy Laboratory.

REFERENCES

1. S. Toda and H. Uchida, Study of liquid film cooling with evaporation and boiling, *Trans. Jap. Soc. Mech. Engrs* **38,** 1830–1848 (1972).
2. Y. Katto and M. Kunishiro, Study of the mechanism of burn-out in boiling system of high burn-out heat flux, *Bull. Jap. Soc. Mech. Engrs* **16,** 1357–1366 (1973).
3. Y. Katto and M. Monde, Study of mechanism of burn-out in a high heat-flux boiling system with an impinging jet, *Proc. 5th Int. Heat Transfer Conf.*, Tokyo, Japan, Vol. 4, pp. 245–249 (1974).
4. Y. Katto and K. Ishii, Burnout in a high heat flux boiling system with a forced supply of liquid through a plane jet, *Proc. 6th Int. Heat Transfer Conf.*, Toronto, Canada, Vol. 1, pp. 435–440 (1978).
5. Y. Katto and M. Shimizu, Upper limit of CHF in the saturated forced convection boiling on a heated disk with a small impinging jet, *J. Heat Transfer* **101,** 265–269 (1979).
6. J. H. Lienhard and R. Eichhorn, On predicting boiling burnout for heaters cooled by liquid jets, *Int. J. Heat Mass Transfer* **22,** 774–776 (1979).
7. T. Ueda, M. Inoue and S. Nagatome, Critical heat flux and droplet entrainment rate in boiling of falling liquid films. *Int. J. Heat Mass Transfer* **24,** 1257–1266 (1981).
8. R. P. Baines, Predicting the critical heat flux for flowing liquid films, M.S. thesis, Massachusetts Institute of Technology, Cambridge, Mass. (1983).
9. R. P. Baines, M. A. El-Masri and W. M. Rohsenow, Critical heat flux in flowing liquid films, *Int. J. Heat Mass Transfer* **27,** 1623–1629 (1984).
10. J. T. Dakin, Vaporization of water films in rotating radial pipes, *Int. J. Heat Mass Transfer* **21,** 1325–1332 (1978).
11. J. T. Dakin, M. W. Horner, A. J. Piekarski and J. Triandafyllis, Heat transfer in the rotating blades of a water-cooled gas turbine, *Am. Soc. mech. Engrs Book No.* H00125, *Gass Turbine Heat Transfer* (1978).
12. R. E. Sundell, W. W. Goodwin, D. M. Kercher, J. C. Dudley and J. Triandafyllis, Boiling heat transfer in turbine bucket cooling passages, *Am. Soc. mech. Engrs* paper No. 80-HT-14 (1980).
13. A. E. Dukler, Fluid mechanics and heat transfer in vertical falling-film systems, *Chem. Engng Prog.* **56,** 1–10 (1960).
14. M. A. El-Masri and J. F. Louis, On the design of high-temperature gas turbine blade water-cooling channels, *J. Engng Pwr* **100,** 586–591 (1978).

15. S. S. Kutateladze and A. I. Leont'ev, Some applications of the asymptotic theory of the turbulent boundary layer, *Proc. 3rd Int. Heat Transfer Conf.*, Chicago, Illinois, Vol. 3, pp. 1–6 (1966).
16. I. A. Mudawwar, Boiling heat transfer in rotating channels with reference to gas turbine blade cooling, Ph.D. thesis, Massachusetts Institute of Technology, Cambridge, Mass. (1984).
17. S. S. Kutateladze, A hydrodynamic theory of changes in boiling process under free convection, *Izv. Akad. Nauk Otdelen. Tekh. Nauk* **4**, 529–536 (1951).
18. N. Zuber, Hydrodynamic aspects of boiling heat transfer, AEUC-4439, Atomic Energy Commission, Oak Ridge, Tenn. (1959).

TRANSFERT THERMIQUE PAR EBULLITION ET FLUX CRITIQUE DANS LES FILMS LIQUIDES TOURNANT A GRANDE VITESSE

Résumé—Des mesures de transfert thermique par ébullition sont effectuées pour des films d'eau dans des canaux radiaux tournants. La courbe d'ébullition ressemble à celle de l'ébullition en réservoir. Le flux de chaleur critique (CHF) augmente avec la pression et avec la vitesse de rotation. On présente un modèle de CHF basé sur le bilan entre les forces de Coriolis et la trainée de vapeur agissant sur les gouttes formées à partir du film. Il permet de rassembler avec succès les données à l'aide d'une seule constante empirique.

WÄRMEÜBERGANG BEIM SIEDEN UND KRITISCHE WÄRMESTROMDICHTE IN SCHNELL ROTIERENDEN FLÜSSIGKEITSFILMEN

Zusammenfassung—Es werden Wärmeübergangsmessungen beim Sieden von Wasserfilmen in rotierenden radialen Kanälen vorgestellt. Man stellt fest, daß die Siedekurve gleich der von Wasser beim Behältersieden ist. Die kritische Wärmestromdichte (CHF) nimmt sowohl mit dem Druck als auch mit der Rotationsgegschwindigkeit zu. Es wird ein CHF-Modell vorgestellt, das auf dem Gleichgewicht zwischen den Coriolis-Kräften und dem Strömungswiderstand des Dampfes basiert. Beide wirken auf die aus dem zerschlagenen Film entstehenden Tropfen ein. Die Daten lassen sich mit Hilfe einer einzigen empirischen Konstanten korrelieren.

ТЕПЛООБМЕН ПРИ КИПЕНИИ И КРИТИЧЕСКИЙ ТЕПЛОВОЙ ПОТОК В ПЛЕНКАХ ЖИДКОСТИ, ВРАЩАЮЩИХСЯ С БОЛЬШОЙ СКОРОСТЬЮ

Аннотация—Исследован теплообмен при кипении водяных пленок в радиально вращающихся каналах. Найдено, что кривая кипения похожа на кривую кипения воды в большом объеме. Критический тепловой поток (КТП) растет с увеличением давления и скорости вращения. Представлена модель КТП, основанная на равновесии между силами Кориолиса и силами, действующими со стороны пара на капли, образованные из раздробленной пленки. Это позволяет обобщить полученные данные с помощью единственной эмпирической постоянной.